Carbon dioxide splitting in a dielectric barrier discharge plasma : a combined experimental and computational study

CO_2 splitting in a dielectric barrier discharge plasma: A combined experimental and computational study

Robby Aerts[a*], Wesley Somers[a] and Annemie Bogaerts[b*]

Abstract: Plasma technology is gaining increasing interest for the splitting of CO_2 into CO and O_2. We have performed experiments to study this process in a dielectric barrier discharge (DBD) plasma in a wide range parameters. The frequency and dielectric material did not affect the CO_2 conversion and energy efficiency, but the discharge gap can have a considerable effect. The specific energy input, has the most important effect on the CO_2 conversion and energy efficiency. We have also presented a plasma chemistry model for CO_2 splitting, which shows reasonable agreement with the experimental conversion and energy efficiency. This model is used to elucidate the critical reactions that are mostly responsible for the CO_2 conversion. Finally, we have benchmarked our results with other CO_2 splitting techniques, and we identified the limitations as well as the benefits and future possibilities in terms of modifications of DBD plasmas for greenhouse gas conversion in general.

Introduction

In recent years, there is a growing interest in the conversion of CO_2 into value-added chemicals or new fuels by means of plasma technology[1–36]. This includes both pure CO_2 splitting into CO_2 and O_2[1–16], as well as the reaction with CH_4 (i.e., so-called dry reforming)[18–32], H_2[33] or H_2O[35,36], yielding syngas and other useful products, such as methanol, formaldehyde and formic acid. Different types of plasmas have been applied for this purpose, but most research is carried out with dielectric barrier discharges (DBD) [1–6,10,18–25,27–30], microwave plasmas[12,15,31] and gliding arc discharges In this paper, we focus on a DBD, as it has a very simple design, which is beneficial for up-scaling, when moving to real applications. This was demonstrated already many years ago for the large scale production of ozone[7,34]. Moreover, it operates at atmospheric pressure, which is again most suitable for practical applications. Finally, it can easily be combined with a packing (of simple dielectric beads and/or catalytic material)[2,21–25], which opens perspectives for the selective production of targeted compounds.

However, before the technology is ready for practical applications, a more systematic investigation of the optimum operating conditions is still needed. In spite of the many papers, as mentioned above, such a systematic investigation for a DBD, focusing on conversion and energy efficiency in a wide range of conditions, has not yet been carried out before. In the present paper, this will be performed for the case of pure CO_2 splitting into CO and O_2.

Some scattered results on CO_2 splitting have been reported already for specific operating conditions[1–3]. Paulussen et al.[1] investigated the effect of flow rate, applied power, frequency and temperature and reported a maximum conversion of 30% at a

flow rate of 0.05 l/min, a power density of 15 W/cm³ and a frequency of 60 kHz. Yu et al.[2] found that adding a dielectric packing results in a rise of the conversion with 8% up to 22.5%, at a plasma power of 35.3 W and a flow rate of 40ml/min. Tagawa et al.[3] proposed a hybrid reactor, i.e., a DBD plasma on the surface of a solid oxide electrolyser cell (SOEC) but they didn't studied the DBD without the SOEC in detail.

Some results are also reported for a mixture of CO_2 with an inert gas, e.g. Ar and N_2[4–6,37–40]. Wang et al.[37] investigated the effect of electrode material and concluded that a Cu electrode has the largest reactivity towards CO_2 decomposition. New ceramic dielectric barriers were developed by Li et al[4,5,39,40] and Wang et al.[6], and gave rise to an increase of the conversion. Zheng et al.[38] studied the effect of voltage and CO_2 concentration, and found that a high voltage and a low CO_2 concentration gave rise to a lower energy efficiency.

Therefore, we strongly believe that a more systematic study is required to improve the performance and also to put a benchmark for other (plasma) technologies. The process we envisage is the following:

$$CO_2 \rightarrow CO + ½\ O_2$$
$$\Delta H_R = 279.8\ kJ/mol = 2.9\ eV/molec\ (at\ 300\ K)$$

This reaction is highly endothermic, so the energy efficiency of the process is a critical issue. However, plasmas can be beneficial for this purpose, compared to other (classical) technologies, because it is well known that the vibrational levels of CO_2 can be efficiently populated in a plasma, and this forms an attractive, energy-efficient route for the dissociation of CO_2, as explained in detail by Fridman[7]. Moreover, plasma technology could also be very powerful for energy storage, which is a topic of great importance, due to the rising contributions of solar and wind energy in the electricity production portfolio. Indeed, these renewable energy sources give rise to peaks in the electricity production, and therefore better storage capacities are urgently needed. Plasma technology is a very powerful candidate for this purpose, because of its high flexibility and its capability to be easily switched on and off[41].

In this paper, we have carried out experiments, varying the applied frequency, power, gas flow rate, dielectric material and discharge gap, focusing on the CO_2 conversion and energy efficiency. Moreover, we have also performed computer

[a] dr. Robby Aerts, MSc. Wesley Somers
Department: Chemistry
Institution: University of Antwerp
Address: Universiteitsplein 1, 2610 Wilrijk, Belgium
E-mail: robby.aerts@uantwerpen.be
[b] Prof. dr. Annemie Bogaerts
Department: Chemistry
Institution: University of Antwerp
Address: Universiteitsplein 1, 2610 Wilrijk, Belgium
E-mail: annemie.bogaerts@uantwerpen.be

simulations, in order to elucidate the underlying mechanisms of the CO_2 splitting process. Finally, we will benchmark our results with other CO_2 splitting techniques, and we will identify the limitations and future possibilities for CO_2 splitting by DBD plasmas.

Results and Discussion

1. Experimental parameter screening

In this section we will discuss the experimental results for the influence of various operating parameters, i.e., frequency, kind of dielectric, discharge gap, electrical power and gas flow rate, on the CO_2 conversion and energy efficiency of the process. Note that we have also investigated the effect of these parameters on the selectivities of the formed products, i.e., CO and O_2, but no influence was observed. The CO and O_2 selectivities were always around 50%, for all conditions investigated. This is like expected, as the underlying chemistry of CO_2 splitting is very simple, i.e., it is determined by the reaction: $CO_2 \rightarrow CO + ½\ O_2$. Some traces of O_3 can be formed (see reaction scheme and calculated number densities in section 2 below), but this could not be detected in our GC analysis.

1.1. Effect of the frequency

The frequency (varied in the range between 6 and 75 kHz at a constant flow rate and plasma power) was found to have a negligible influence on the conversion and energy efficiency. However, the plasma appears more filamentary at high frequency (75 kHz) compared to low frequency (6 kHz), as is illustrated in Figure 1. In this study, we therefore apply a fixed frequency of 23.5 kHz, which is the energetically optimal resonance frequency of the power generator used.

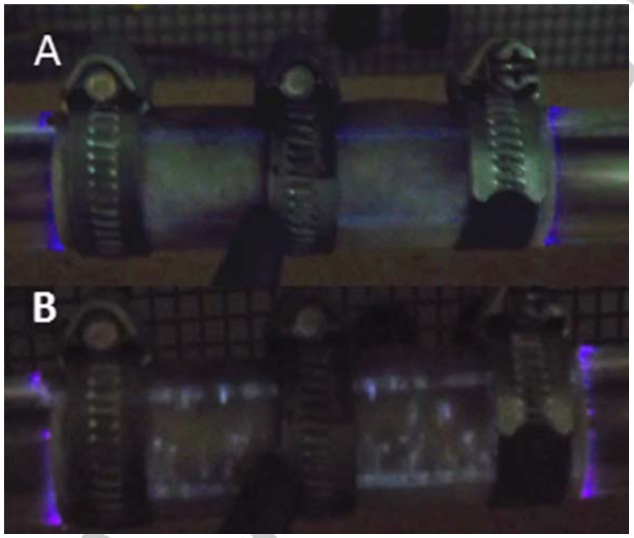

Figure 1: *Pictures of the DBD plasma at a frequency of 6 kHz (A) and 75 kHz (B), illustrating the difference in filamentary character.*

1.2. Effect of the dielectrics

We performed several experiments, for different discharge gaps and a wide range of operating conditions, comparing quartz and alumina (99.7% Al_2O_3, Ceratec) as dielectrics, but we observed no significant differences on the performance of the CO_2 splitting. Figure 2 presents the conversion and energy efficiency for both dielectrics, as a function of specific energy input (SEI), for a discharge gap of 1.8mm (see also the experimental section below). The SEI is defined here by changing the gas flow rate between 10 and 500 ml/min, while keeping the applied power constant at 80W. This results in a plasma power of 35W ± 3W for quartz and 39W ± 1W for alumina. The conversion increases with SEI , as expected, and reaches values up to 35% at the highest values of SEI investigated (around 225 J/cm^3, which corresponds in this case, i.e., for a power of 39W ± 1W, to a gas flow rate of 10 ml/min, or a quite long gas residence time of 44s). The energy efficiency, on the other hand, drops upon higher SEI, which is also like expected (see the formulas in the experimetal section below). When reaching a conversion of 35%, the energy efficiency is only 2%. A higher energy efficiency of 8% could be reached at an SEI of 25 J/cm^3, but this corresponds to a very low conversion of only a few %. Hence, there is a clear trade-off between conversion and energy efficiency. Depending on the targeted application and the boundary conditions (e.g., use of sustainable electricity), the one or the other can thus be optimized or a compromise between both can be sought.

Although virtually no difference was observed between quartz and alumina dielectrics on the conversion and energy efficiency (except for some minor differences in the lower region of the SEI , i.e., below 100 J/cm³), the use of alumina instead of quartz has some advantages in terms of fabrication, and it is more resistant against arc formation and high temperature (melting point of 2054 °C vs. 1470 °C for quartz)[42]. It is worth to mention that in literature some more sophisticated dielectrics, like $Ca_{0.8}Sr_{0.2}TiO_3$[6] and $Ca_{0.7}Sr_{0.3}TiO_3$ with 0.5 wt.% $Li_2Si_2O_5$[4,39], were reported to enhance the CO_2 conversion and/or energy efficiency, because they increase the density of the filaments in the plasma. A more thorough discussion about this effect will be made in section 4.

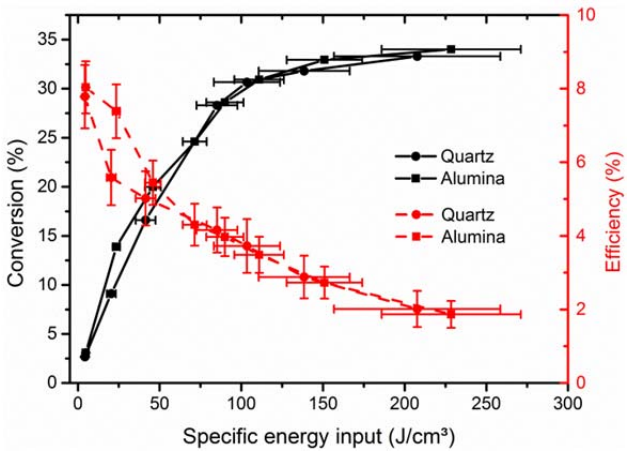

Figure 2: *Effect of the dielectric on the conversion (black curves, left axis) and energy efficiency (red curves, right axis), as a function of the SEI. The calculation of the error bars is based on the uncertainties of the power, the flow rate and the GC measurements. The error bars of the conversion in the y-direction are smaller than 1% and therefore not visible.*

1.3. Effect of the discharge gap

The influence of the discharge gap on the conversion and energy efficiency is presented as a function of the SEI in Figure 3. We use here a quartz dielectric, because it is transparent and thus allows visible observation. The SEI is again varied by adjusting the gas flow rate in the range between 10 and 500 ml/min, at a constant plasma power of 35W ± 3W.

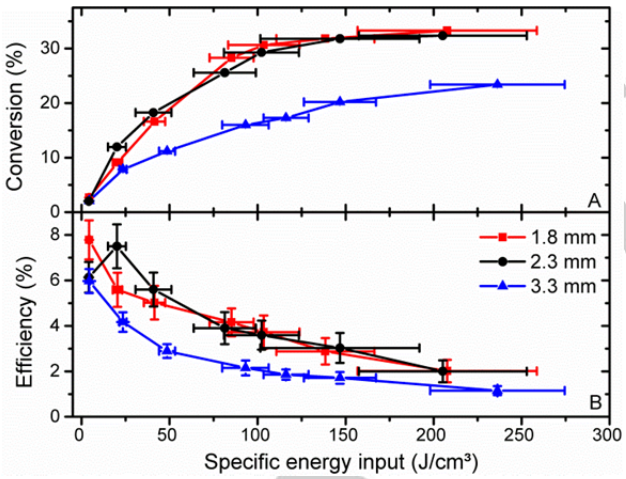

Figure 3: *Effect of the discharge gap on the conversion (Figure A) and energy efficiency (Figure B), as a function of the SEI . The calculation of the error bars is based on the uncertainties of the power, the flow rate and the GC measurements. The error-bars of the conversion in the y-direction are smaller than 1% and therefore not visible.*

The gaps of 1.8 mm and 2.3 mm yield roughly the same conversion and energy efficiency, but the gap of 3.3 mm results in a clear drop in conversion and hence also in the energy efficiency. A larger gap of 4.5 mm was also tested but the discharge was only ignited at the sharp edges of the foil electrode and thus no stable volume discharge was established.

Note that for a fixed SEI (and hence gas flow rate and power) the residence time will be longer, and the power density will be lower, for the larger discharge gaps, due to the larger volume (i.e., the reactor volume is 7.4 cm^3, 9.2 cm^3, and 12.3 cm^3, for the gaps of 1.8, 2.3 and 3.3 mm). Indeed, for instance at a SEI of 100 J/cm^3, the residence times will be 22.1, 27.4 and 36.8, while the power densities will be 4.7, 3.7 and 3.2, in the gaps of 1.8 mm, 2.3 mm and 3.3 mm, respectively. It appears that this longer residence time and lower power density compensate each other for the gaps of 1.8 and 2.3 mm, but for the 3.3 mm gap, the lower power density seems dominant.

Therefore, we make a more detailed analysis of the effect of the discharge gap by looking at the Lissajous plots, presented in Figure 4. Note that the total surface area is the same, as the latter is determined by the plasma power (±35W), but nevertheless, there are distinct differences in the three Lissajous plots. Indeed, as the gap increases, a larger applied voltage is necessary to maintain the discharge (i.e., 13, 14 and 15 kV_{pp} for the gaps of 1.8, 2.3 and 3.3 mm, respectively). Moreover, as the plasma power is the same, this increase in applied voltage is compensated by a drop in peak-to-peak charge.

The difference in applied voltage and charges for the three discharge gaps is, however, gradual, and the same for the gaps of 1.8, 2.3 and 3.3 mm, and therefore it cannot explain why virtually no difference in conversion and energy efficiency was observed between 1.8 and 2.3 mm, whereas the difference was quite striking for the 3.3 mm gap. Therefore, to fully understand the effect of the gap on the conversion, we calculate the capacitance for the dielectric (C_d) and the gap (C_g), as well as the capacitance of the reactor without plasma (C_{cell}) and the effective capacitance during the plasma-on stage (C_{eff})[43].

$$C_d = \frac{2\pi\varepsilon_0\varepsilon_d L}{\ln(r_{outer}/r_{inner})} \quad \text{(E1)}$$

$$C_g = \frac{2\pi\varepsilon_0\varepsilon_g L}{\ln(r_{inner}/r_{rod})} \quad \text{(E2)}$$

$$C_{cell} = \frac{1}{C_d} + \frac{1}{C_g} \quad \text{(E3)}$$

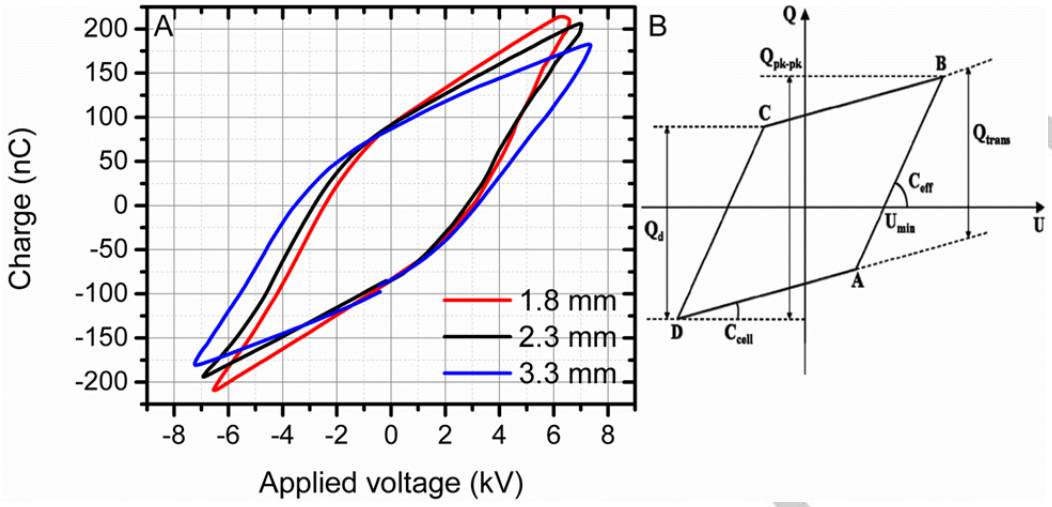

Figure 4: *Lissajous plots for the three different discharge gaps, at a plasma power of ±35 W, with a quartz dielectric (A), and schematic diagram of the Lissajous plot, explaining all the quantities that can be deduced from it (see text) (B).*

In these formula $\varepsilon_0 = 8.854 \times 10^{-12}$ Fm^{-1} is the permittivity of vacuum, $\varepsilon_g = 1.000922$ is the relative permittivity of CO_2 and $\varepsilon_d = 3.8$ for quartz[43,44]. Furthermore, L is the length of the plasma (90 mm; see above), r_{inner} and r_{outer} are the inner and outer radii of the dielectric tube (i.e., constant in the three cases) and r_{rod} is the radius of the high voltage electrode (rod), which is varied as 5, 6 and 6.5 mm (see above). This results in a constant C_d of 67 pF, whereas Cg varies from 21 pF for the smallest gap (1.8 mm) to 16 pF for the gap of 2.3 mm, and 10 pF for the largest gap of 3.3 mm.

These values should be compared with the slopes of lines AB and CD from the Lissajous plots of Figure 4, which represent the effective capacitance C_{eff} during the discharge-on phase, when the gas breakdown occurs in the gap and the plasma is ignited. The slope of these lines should be equal to C_d for a fully bridged gap[45]. In our case, C_{eff} is determined to be 56 pF for the gaps of 1.8 and 2.3 mm, and 40 pF for the gap of 3.3 mm. This is clearly lower than the capacitance of the dielectric quartz tube (C_d = 67 pF; see above), especially for the largest gap, indicating that the discharge gap is not fully bridged. Tu *et al.* indeed reported that C_{eff} depends on the spatial distribution of the discharge across the gap over a half-period of the applied voltage[25]. Hence, it can be concluded that the total plasma volume (i.e., the volume occupied by the streamers) is much smaller than the total volume of the plasma reactor, especially for the largest gap.

This reduced formation of streamers is clearly visible in the electric current waveforms, illustrated in Figure 5. Comparing the waveforms of the 1.8 and 2.3 mm gaps tells us that the absolute values of the current are somewhat lower in the 2.3 mm gap, which is correlated with the slightly lower peak-to-peak charges, illustrated in the Lissajous plots. This trend is also continued, and even more striking, for the gap of 3.3 mm, but on top of that, the streamer frequency is clearly reduced, compared to the gaps of 1.8 and 2.3 mm.

To conclude, the gaps of 1.8 and 2.3 mm yield more or less the same CO_2 conversion and energy efficiency, because they exhibit the same streamer behavior. On the other hand, the larger gap of 3.3 mm results in a clearly lower CO_2 conversion and energy efficiency (cf. Figure 3 above), as less streamers are formed for a fixed SEI , giving rise to a lower effective plasma volume, and therefore a reduced possibility for CO_2 conversion. Moreover, the streamers seem to have lower peak currents, which corresponds to a drop in the electron density, due to the following relation:

$$n_e = \frac{J}{E \mu_e e} \qquad \text{(E4)}$$

where J is the current density, E the electric field and μ_e the electron mobility. Consequently, the lower electron density results in a lower CO_2 conversion, because of the drop in electron impact reaction rates[10]. Finally, an increasing gap distance gives rise to a reduced electric field strength (E/N), and this results in a drop in the average electron energy in the discharge. This lower electron energy (or reduced electric field) will affect the fraction of energy transferred to the various types of collisions[10,46]. Nevertheless, as the gap of 3.3 mm clearly shows a lower conversion and energy efficiency than the gaps of 1.8 and 2.3 mm, we can conclude that the reduced streamer density in the 3.3 mm gap is more important in determining the lower conversion and energy efficiency than the latter two effects.

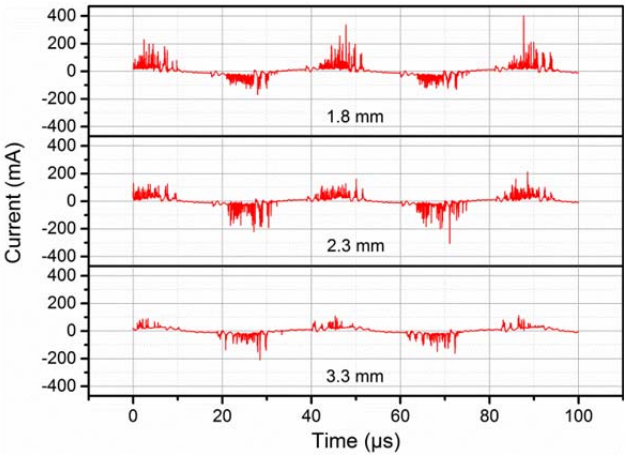

Figure 5: *Comparison of the electric current waveforms for the three different discharge gaps at a plasma power of ±35 W, with a quartz dielectric, illustrating the reduced streamer formation for the gap of 3.3 mm.*

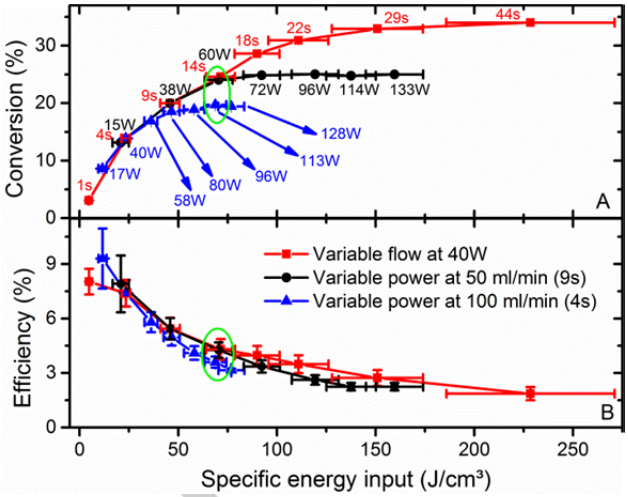

Figure 6: *Effect of the gas flow rate (or residence time) and plasma power on the conversion (Figure A) and energy efficiency (Figure B), plotted as a function of the SEI, using alumina dielectrics. The corresponding values of plasma power, resulting in certain SEI values at the fixed gas flow rates of 50 and 100 ml/min (black and blue curves), as well as the corresponding values of the residence time, resulting in certain SEI values at a fixed plasma power of ±40 W (red curve), are also shown in Figure A. The calculation of the error bars is based on the uncertainties of the power, the flow rate and the GC measurements. For the sake of clarity, the error bars are only presented for the energy efficiency. The green circle in Figure A indicates the conditions plotted in Figure 7 below.*

1.4. Effect of the electric power and gas flow rate

As indicated by the formula in the experimental section, the SEI in the plasma system is defined by both the gas flow rate and the plasma power. In literature, the SEI is often used as a major determining factor for the conversion and energy efficiency, and therefore, the conversion and energy efficiency are often plotted as a function of SEI[8,18,36,47]. However, we observed that the same values of SEI, but defined by different combinations of plasma power and gas flow rate, can result in a different conversion. Therefore, in this section we investigate the influence of gas flow rate (or residence time) and plasma power on the CO_2 conversion and energy efficiency separately. To our knowledge, such a separate study is never published before.

In Figure 6 the conversion and energy efficiency are plotted vs SEI, for different values of residence time (or gas flow rate) at fixed plasma power (red curve), and for different values of plasma power, at fixed gas flow rates (blue and black curves). The figure clearly indicates that these two parameters affect the SEI, and therefore the CO_2 conversion and energy efficiency, in a different way. In all cases, the conversion first increases with SEI, but then saturates to a maximum value, which appears to be different in the different cases. A low plasma power (40 W) with a low gas flow rate (of 10 ml/min, corresponding to a long residence time of 44 s) gives rise to a maximum conversion (see red curve). The same SEI can also be obtained with a higher plasma power and higher gas flow rate (or shorter residence time), and this obviously results in a lower maximum conversion, as is clear from the black and blue curves. Hence, the flow rate (or gas residence time) seems to have a more pronounced effect on the conversion than the plasma power. The same effect is visible for the energy efficiency, but it is less pronounced. To our knowledge, this effect has not yet been reported before. It suggests that by a proper tuning of plasma power versus gas flow rate, we can increase the conversion and energy efficiency at a certain SEI, which is very promising. However, this effect is only observed for high values of SEI (above 100 J/cm³), which unfortunately gives rise to a low energy efficiency.

To compare the three cases presented in Figure 6 from the electrical point of view, the current and voltage waveforms for three distinct combinations of plasma power and gas flow rate, resulting in nearly the same SEI of 70 J/cm^3, are shown in Figure 7. We observe more streamers and especially higher current values in the case of a high power and high flow rate (upper panel) than in the case of a low power and low flow rate (lower panel), which is quite logical. Nevertheless, the first condition gives rise to a lower conversion. This indicates that the longer residence time, which arises from the lower gas flow rate (lower panel), has a more pronounced effect on the conversion (and hence energy efficiency) than the higher power (and thus higher current and higher streamer intensity). Indeed, a longer residence time means that the CO_2 molecules can stay longer within the streamers, and this seems more important for the conversion than the higher streamer intensity (or electron density), for the same SEI.

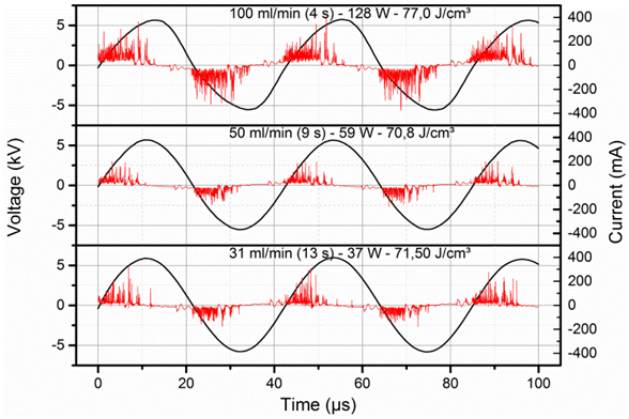

Figure 7: *Comparison of the voltage and electric current waveforms for three different combinations of plasma power and gas flow rate (or residence time), yielding a similar SEI (cf. the green circle indicated in Figure 7 above).*

2. Modelling the plasma chemistry of CO_2 splitting

In this section we extend our model published previously[10] to longer residence times, by simulating a large number of consecutive pulses (i.e., microdischarge filaments or streamers) at an arbitrarily chosen frequency of 34.4 Hz (see also description of the model), until a given residence time is reached. As indicated in Section 1 above, the effective volume occupied by the sum of all individual micro-discharges is much smaller than the total plasma reactor volume. Therefore, the power density used as input in our model, from which the SEI is calculated, is multiplied by a factor 7, to account for this. Note that we don't know the exact value of the effective plasma volume occupied by the streamers, so this factor 7 is chosen somewhat arbitrarily, because it yields reasonable agreement between the calculated and measured values for the CO_2 conversion (see below). Nevertheless, even if this factor can be considered as a kind of fitting parameter, it does have a physical meaning, as demonstrated by Motret et al.[48,49], and even if the quantitative calculation results might be dependent on this factor, the qualitative trends predicted by the model can still be validated in this way, and the validated model can then subsequently be used to elucidate the underlying plasma chemistry. The latter will be illustrated in this section, based on a reduced plasma chemistry, which still describes the essential processes for the CO_2 conversion, and which will also be very useful for the development of time-consuming 2D or 3D plasma chemistry models.

2.1. Validation of the model

Figure 8 illustrates the comparison of the calculated conversion with measured values for different powers and gas flow rates (cf. Figure 6 above), as a function of SEI. A very good agreement is reached for SEI values up to 100 J/cm³. Above 100 J/cm³ the model does not show saturation, like in the experiments, but the experimental data also yield different degrees of saturation, depending on the combination of power and gas flow rate, as explained in detail in section 1.4 above. On the other hand, the energy efficiency at these high SEI values is very low (see section 1.4 above), and the residence time becomes quite long, so these conditions are probably not attractive anyway. Therefore, we may conclude that the agreement between model and experiments is reasonable, at least in the SEI region of most practical interest. Furthermore, in Aerts et al.[10] we checked that the calculated electron density and temperature in the model are in the correct order of magnitude, compared with literature data. Hence, we may conclude that the model is sufficiently realistic to be used for elucidating the underlying chemical pathways of CO_2 splitting.

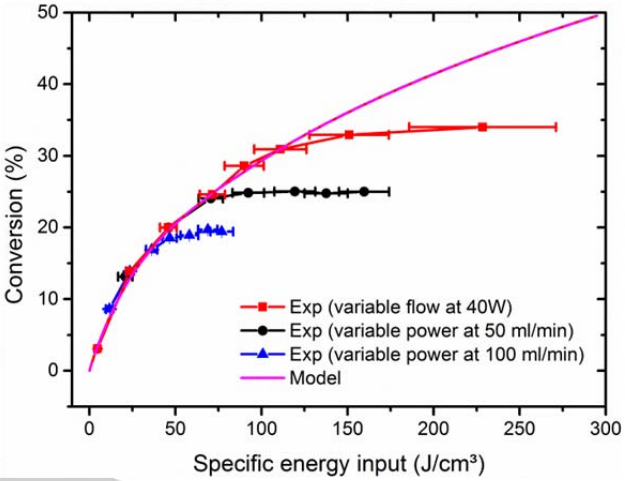

Figure 8: *Comparison of the calculated and measured values for the conversion, as a function of the SEI. Note that the power density, and hence the SEI, used in the model is multiplied by a factor 7, to account for the lower volume occupied by the streamers (see text). The calculation of the error bars is based on the uncertainties of the power, the flow rate and the GC measurements. The error-bars in the y-direction are smaller than 1% and therefore not visible.*

2.2. Reduced chemistry set for CO_2 splitting

As also mentioned in the experimental section, the complete model contains 42 species which interact with each other in 501 chemical reactions. This will be prohibitively long for 2D and 3D plasma models. Therefore, we have reduced the chemistry set described in Aerts et al.[10], based on the most important production and loss processes of our full model, so that it only includes the most critical plasma species and reactions for the CO_2 splitting (see below).

Figure 9 illustrates the comparison between the conversions, calculated by the full model and the reduced model, as a function of SEI in the model. A good agreement is reached in the lower range of the SEI, yielding a limited conversion of CO_2 (i.e., up to 15%), for the reasons discussed below. When the conversion rises above 15%, the chemistry becomes more complex due to the higher concentrations of CO and O_2. To obtain a good correlation in the higher SEI range, too many reactions have to be included again, so that there is no significant speed-up, compared with the full model. Therefore, for higher conversions, we recommend to use the full chemistry set. Only 9 different species are included in this reduced model, i.e., CO_2, CO, O, O_2 and O_3 as neutral species, and CO_2^+, O_2^-, O^- and the electrons as charged species. Indeed, we do not

include vibrationally or electronically excited levels of the molecules as separate species. Although vibrationally excited CO_2 molecules play a critical role in the CO_2 splitting in microwave or gliding arc plasmas[7,50], their contribution in DBD plasmas is of minor importance[7,10,50]. On the other hand, these excited species play a role in the consumption of the electron energy. To compensate for this, we included some dummy reactions with no change in chemical species, which account for the energy loss in the electron energy equation.

The only electron impact ionization process included in the reduced model is the ionization of CO_2 to CO_2^+ (reaction 1 in Table 1), as this reaction was found to be much more important than dissociative ionization of CO_2[10]. Moreover, the ionization processes of CO and O_2 are also less important, as long as the conversion is not too high. This will of course limit the validity of the reduced model to low conversions (i.e., up to 15%; see Figure 9 below), but including these ionization processes will increase the number of species and reactions. Hence, this shows the trade-off between complexity (or calculation time) and validity of the model. Furthermore, charge transfer processes between ions are not considered either, as the role of ions to the actual splitting of CO_2 is almost negligible[10]. The only reactions of the CO_2^+ ions included are recombination with electrons and with O_2^- ions (reactions 11, 12 in Table 1).

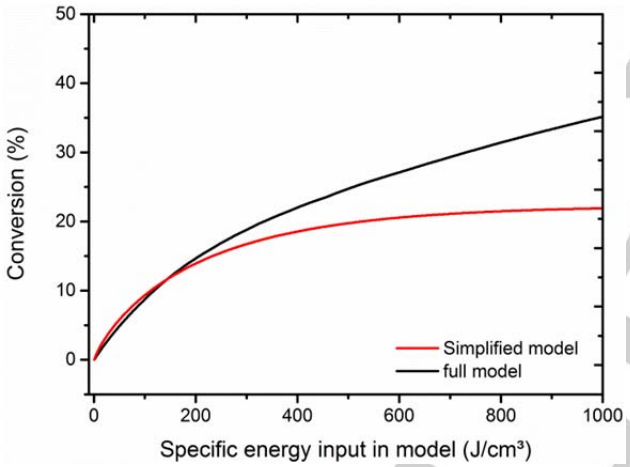

Figure 9: *Comparison of the conversion, calculated with the simplified model and the full model from Aerts et al.*[10]*, as a function of SEI in the model.*

Three electron impact dissociation reactions are incorporated, i.e., for CO_2, O_3 and O_2 (reactions 2, 4, 5 in Table 1). The dissociation of CO can be neglected because it requires 1069.2 kJ/mol, while the dissociation of CO_2 requires 529.8 kJ/mol[38]; due to this energy difference the total rate of CO dissociation, as calculated by the full model, is much lower than the rate of CO_2 dissociation, especially for lower conversions (below 15%). Furthermore, three electron attachment processes are considered, i.e., dissociative attachment to CO_2 and O_2, as well as (three-body) attachment to O_2, producing O^- or O_2^- ions, respectively (reactions 3, 6, 7 in Table 1). As only a limited number of reactions are included for these negative ions in the simplified model, this is another reason why the model should not be used for conversions above 15%. On the other hand, the electron attachment reactions with O_2 are essential, even in this reduced chemistry set, as they are faster than the one with CO_2 and they will induce a drop in electron density, resulting in a flattening in the CO_2 conversion upon rising SEI, which is also observed experimentally (see above), because less electrons will be available for direct splitting of CO_2. Furthermore, three electron detachment reactions are included, i.e., by O^- upon collision with CO, O_2 and O_3 (reactions 8-10). The O_2^- ions, on the other hand, are neutralized by recombination with CO_2^+ ions (reaction 12; see above).

Finally, some chemical reactions between the neutral species are incorporated (reactions 13-17). The O atoms recombine almost completely to O_2 by reaction 13, although some O atoms give rise to the production of O_3 as well, predominantly by reaction 14. Moreover, some O atoms can recombine with CO to produce CO_2 (reaction 16), especially at high conversions and a long residence time. Indeed, this reaction will become important if the density of atomic oxygen is high enough. In addition, a rise in the supplied energy will also increase the rate of this reaction, e.g., when a large fraction of O atoms is in excited levels or at higher gas temperature[7]. That is the reason why in thermal (or warm) plasmas used for CO_2 splitting, the gas needs to be quenched (cooled) rapidly to prevent the backward reaction (i.e., recombination of CO and O, to form CO_2 again) to occur[7]. At our conditions, the gas temperature did not increase during splitting, i.e., the gas temperature remains close to room temperature, and therefore, this reaction will be less important, at least for not too long residence times (see below). Hence, once the CO molecules are formed, they will be rather stable in the plasma. On the other hand, we do observe a certain balance in our model between O_3 and O_2, determined by reactions 13-15,17. It should be mentioned, however, that especially the rate constants for the three-body reactions adopted from literature show a variation between different publications and thus the exact O_3/O_2 ratio obtained by the model is subject to uncertainties. Experimental measurements of the O_3 density would give vital information to understand the balance between O_2 and O_3 in the splitting of CO_2. However, we were not able to detect O_3 with our GC setup. The reactions included in the reduced model, as well as the corresponding rate coefficients and the references where these data are adopted from, are listed in Table 1, and a schematic diagram of the reaction scheme is presented in Figure 10.

Table 1: Reactions included in the reduced chemistry model, as well as the corresponding rate coefficients and the references where these data are adopted from. The rate coefficients are in units of $cm^3\ s^{-1}$ for the two-body reactions, and in $cm^6\ s^{-1}$ for the three-body reactions.

	Reaction	Rate coefficient	Ref.
1	$e^- + CO_2 \rightarrow CO_2^+ + 2\ e^-$	5.4×10^{-11}	a [10]
2	$e^- + CO_2 \rightarrow CO + O + e^-$	5.8×10^{-11}	a [10]
3	$e^- + CO_2 \rightarrow CO + O^-$	7.0×10^{-12}	a [10]
4	$e^- + O_3 \rightarrow O + O_2 + e^-$	2.0×10^{-9}	a [10]
5	$e^- + O_2 \rightarrow O + O + e^-$	2.0×10^{-9}	a [10]
6	$e^- + O_2 \rightarrow O + O^-$	4.0×10^{-11}	a [10]
7	$e^- + O_2 + M \rightarrow O_2^- + M$	3.0×10^{-30}	a [10]
8	$O^- + CO \rightarrow CO_2 + e^-$	5.5×10^{-10}	[51]
9	$O^- + O_2 \rightarrow O_3 + e^-$	1.0×10^{-12}	[52]
10	$O^- + O_3 \rightarrow O_2 + O_2 + e^-$	3.0×10^{-10}	[53]
11	$e^- + CO_2^+ \rightarrow CO + O$	6.5×10^{-7}	[54]
12	$O_2^- + CO_2^+ \rightarrow CO + O_2 + O$	6.0×10^{-7}	[55]
13	$O + O + M \rightarrow O_2 + M$	5.2×10^{-35} exp(900/T[K])	[56]
14	$O + O_2 + M \rightarrow O_3 + M$	4.5×10^{-34} $(T[K]/298)^{-2.70}$	[57]
15	$O + O_3 \rightarrow O_2 + O_2$	8.0×10^{-12} exp(−17.13/T[K])	[57]
16	$O + CO + M \rightarrow CO_2 + M$	1.7×10^{-33} exp(-1510 [K]/T)	[58]
17	$O_3 + M \rightarrow O_2 + O + M$	4.1×10^{-10} exp(−11430/T[K])	[51]

[a]Rate coefficient calculated by an online Boltzmann solver in the model, at initialization conditions of pure CO_2.

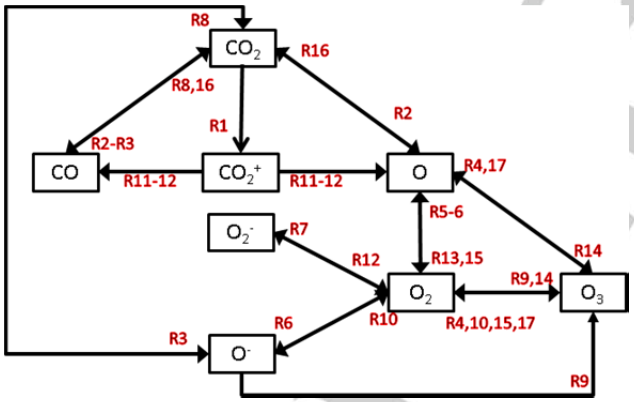

Figure 10: *Reaction scheme, illustrating the chemistry of CO_2 splitting and further reactions, as predicted by the reduced model.*

It is clear from Figure 10 that the actual splitting of CO_2 is quite straightforward. The most important reactions for CO_2 splitting are electron impact dissociation (to form CO and O atoms (R2)), electron impact ionization (to form CO_2^+ ions (R1), which will further dissociatively recombine with electrons or O_2^- ions into CO and O and/or O_2 (R11, R12)), and electron dissociative attachment (to form CO and O^- ions (R3)). These three mechanisms contribute typically for 43%, 46% and 11% to the CO_2 splitting. As mentioned above, the CO molecules are relatively stable and will only react further at longer residence times or higher O densities; they can recombine with O^- ions (electron detachment of O^- (R8)) or O atoms (R16) to form again CO_2. To analyse the importance of these backward reactions as a function of the residence time, the time averaged rates (i.e., averaged over one pulse) are plotted in Figure 11, together with the time averaged rates of the dominant loss processes of CO_2, i.e., electron impact ionization, dissociation and dissociative attachment.

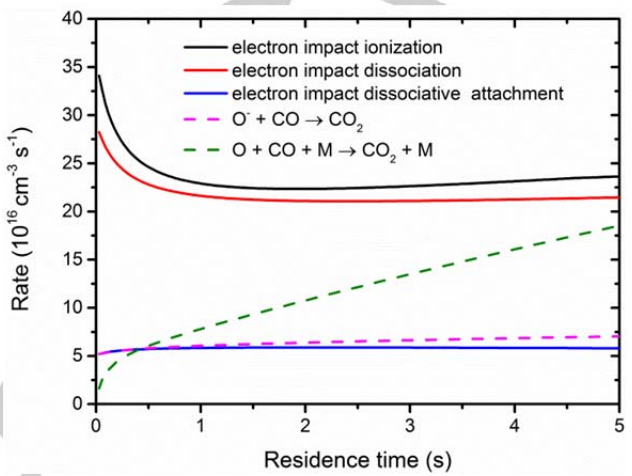

Figure 11: *Time averaged rates of the dominant loss processes of CO_2 (full lines) and of the backward reactions of CO with O and O^- (dashed lines) calculated with the simplified model, as a function of residence time, for a SEI of 129 J/cm³.*

At a residence time of 0.5 s, both backward reactions are more or less equally important with a rate of $6\times10^{16}\ cm^{-3}\ s^{-1}$, but the sum of their rates is a factor 4.5 lower than the sum of the rates of the main loss mechanisms of CO_2 (i.e. ionization, dissociation and dissociative attachment). However, at a residence time of 5 s the total rate of the backward reactions is only a factor 2 lower than the total loss rate, indicating that the backward process then becomes indeed important. It is clear that the reaction with O^- ions has a more or less constant rate of $6\times10^{16}\ cm^{-3}\ s^{-1}$, independent of the residence time, which is caused by the constant production of O^- ions from electron impact dissociative attachment with CO_2 (R3). In contrast, the rate of the reaction with O atoms increases by almost an order of magnitude, up to a value of $2\times10^{17}\ cm^{-3}\ s^{-1}$ at 5 s. The latter can be explained by the increasing O_2 density and therefore, the increasing production of O atoms by electron impact dissociation of O_2 (R5). Overall, integrated over the residence time of 5 s, the total contribution from recombination of CO with O atoms to the CO_2 production is 65% while the recombination with O^- ions only contributes for 35%. Hence, we can distinguish two major phenomena which cause the flatting of the conversion at long residence times, or high values of the SEI. The first one is the drop in the electron density due to electron attachment with oxygen. The second one is the increasing contribution of the backward reaction, i.e. the recombination of O atoms with CO to form again CO_2.

At shorter residence times, however, the O atoms will almost immediately recombine into O_2 or O_3, as mentioned above (R13, R14), and there are several other reactions between O, O_2 and

O_3 as well (sometimes also involving the negative ions; i.e., R4-R7, R9, R10, R15, R17). Therefore, most freedom to influence the splitting process can be found in the balance of $O/O_2/O_3$. Moreover, introducing H-containing gases, like H_2 or CH_4, can further control the production of O_2 by consumption of O atoms[59].

To conclude, the selectivity towards CO will always be close to 50%, whereas the selectivity towards O_2 was predicted in the model to be between 45 and 50%, depending on the O_3 production (and keeping in mind the uncertainties in the three-body rate coefficients, as mentioned above). The question is whether O_2 or O_3 would be the most valuable product. Based on the chemical reactivity, O_3 is more favorable, but due to its high reactivity, the storage of O_3 is not straightforward and therefore an on-site production would be beneficial when O_3 is intended to be produced for bleaching or oxidizing purposes[60].

Finally, the calculated number densities of the molecules included in the model are plotted as a function of residence time in Figure 12(A), for a SEI of 129 J/cm³. It is clear that the CO_2 density gradually drops, while being converted into CO and O_2, and some fraction of O_3. The densities of the other species included in the model (i.e., the O atoms and the various ions) are negligible at these long time-scales; however, their densities are plotted, together with the molecule densities, as a function of time during 5 consecutive microdischarge pulses (mimicking the filaments in the DBD reactor) in Figure 12(B), for the same SEI value. Note that we use a logarithmic x-axis, to clearly illustrate the temporal behavior of the ions during and after one pulse. It is clear that the densities of CO, O_2 and O_3 increase (more or less) stepwise at each pulse, while the CO_2 density slightly drops. The densities of the O atoms, the various ions and the electrons rise during each pulse, but they decay again before the next pulse is reached. The decay time is the longest for the O atoms, whereas the electrons and the various negative ions become completely negligible, long before the next pulse starts.

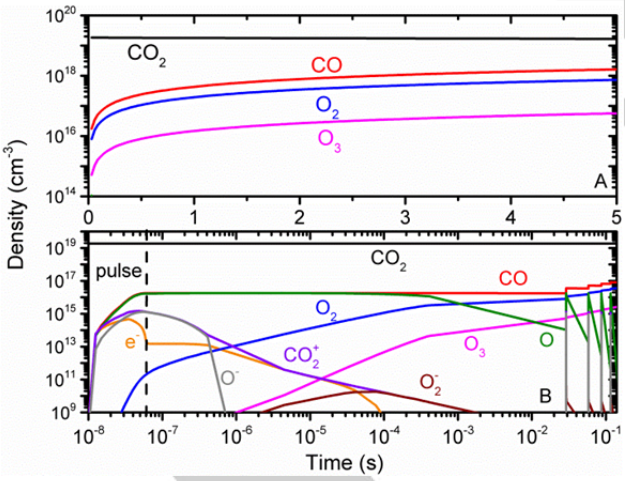

Figure 12: *Calculated molecule densities as a function of residence time (A), and densities of all plasma species included in the simplified model, as a function of time during 5 consecutive microdischarge filaments (B), for a SEI of 129 J/cm³.*

3. Theoretical energy cost versus actual energy cost

In our experiments, the conversion was at maximum around 35%, but this was reached at a high SEI above 200 J/cm^3, and therefore it corresponds to a low energy efficiency of only 2%. A maximum energy efficiency of 8% could be obtained at low SEI (~ 25 J/cm^3), but at the expense of the conversion, which was only a few % in this case. An important remark is that the energy efficiency reported in our work, as well as in literature (see section 4 below), is calculated with respect to the plasma power. Therefore, we should refer to it as the "energy efficiency of the plasma" or the "theoretical energy efficiency". Indeed, the plasma power is typically around 50% lower than the applied electrical power in a DBD reactor, due to losses in the high voltage power source and the cables (reflection, heating, zero load power requirements,…). As a consequence, the actual energy efficiency of the process will still be lower, or vice versa, the actual energy cost will be higher.

Figure 13 shows a comparison of the energy cost and the energy efficiency, as calculated from the electrical power and the plasma power, as a function of the SEI. It is clear that the actual energy cost, calculated from the electrical power, is at least 50% higher (see black dashed line) and therefore, the actual energy efficiency (red dashed line) is also at least 50% lower, compared to the theoretical energy cost and energy efficiency (black and red solid lines).

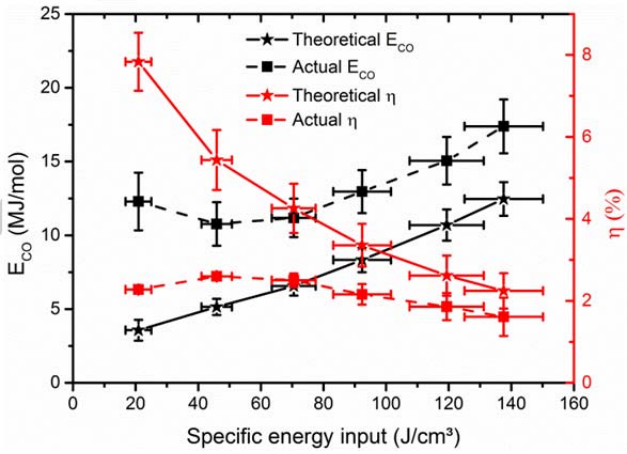

Figure 13: *Energy cost (black curves; left axis) and energy efficiency (red curves; right axis), as calculated from the electrical power ("actual"; dashed lines) and from the plasma power ("theoretical"; solid lines), as a function of the SEI, using alumina dielectrics and a constant flow rate of 50ml/min.*

At higher values of the SEI, the difference between actual and theoretical energy cost and energy efficiency is somewhat lower than at low SEI values. This can be explained by the zero load power of the power source, which is ±40W in our experiments, independent of the applied power. Hence, the power loss at higher applied power is thus relatively smaller than at lower applied power.

In the present paper, we focus on the energy efficiency of the plasma process itself, like is typically done in plasma studies

in literature. Nevertheless, the total electrical power consumption must be kept in mind, especially when different plasma sources are compared, and certainly also when benchmarking with other CO_2 conversion technologies.

4. Feasibility of CO_2 splitting by DBDs, and benchmarking with other techniques

The purpose of this study is to identify the possibilities and drawbacks of CO_2 splitting by DBDs, by investigating the effect of various operating conditions. We found that a proper tuning of power versus gas flow rate can increase the conversion and energy efficiency at a certain SEI, but this is only observed for high values of SEI (above 100 J/cm³), which yields a low energy efficiency anyway. Reducing the discharge gap can enhance the filament formation, and therefore the conversion and energy efficiency, but this enhancement was only observed for larger gaps. Changing the dielectrics from quartz to alumina did not show any effects on the conversion and energy efficiency, although more sophisticated dielectric materials did show drastic changes, as reported in literature[4–6,39,40] (see below).

To benchmark our results, we compare them in Table 2 with some studies published for CO_2 splitting by several types of plasmas, as well as with classical thermal splitting. Note that we can only compare with other studies for pure CO_2 splitting, as other gas mixtures (e.g., with inert gases) affect the conversion and energy efficiency[4,5,27,37–40,61], and we don't want to draw the wrong conclusions. We focus on the maximum conversion, the energy efficiency (if this could be calculated from the literature data) and the gas flow rate. The latter is also relevant because it gives an idea about the scalability and industrial applicability of the process. Indeed, a high conversion at a very low flow rate and long residence time is not of interest for industrial applications.

Detailed, systematic studies for CO_2 splitting in a pure CO_2 mixture, presenting values for both conversion and energy efficiency in a DBD, appear to be very scarce in literature. The most detailed study up to now was presented by Paulussen et al.[1] and Yu et al.[2]. Paulussen et al.[1] found a maximum conversion of 30% at a flow rate of 0.05 l/min, a power density of 15 W/cm³ and a frequency of 60 kHz. However, they did not report the plasma power or the energy efficiency. Yu et al.[2] reported a maximum conversion of 12.5% at a constant flow rate of 40 ml/min, hence somewhat lower than our results. Their maximum energy efficiency was around 3.5%, which is also somewhat lower than in our case. However, we should point out that the reactor used in their work had a very large gap (4 mm) to study the effect of a packing material. Therefore, we should compare these results with our results for a gap of 3.3 mm (see Figure 3 above), showing a maximum conversion of 25% and a maximum energy efficiency of 6%.

A microwave discharge seems very promising for CO_2 splitting[7,12,13,15,50,62]. In the 1970s, Fridman and coworkers reported energy efficiencies up to 80-90%, when operating in the supersonic flow regime, with a flow rate in the order of 5-50 ml/min and a static pressure between 0.02 and 0.05 atm[7]. The highest energy efficiency reported recently, for similar conditions, was around 60%[13]. Note, however, that these results were obtained at reduced pressure (0.2 bar), which is not so practical for high-throughput processing of exhaust gases, and it will increase the total energy cost, as higher pressures are required for gas storage. Furthermore, it was also reported[8,12,15] that increasing the pressure can lead to a significant drop in the energy efficiency. Therefore, in this benchmarking, we want to compare with microwave results obtained at atmospheric pressure, which allows a more fair comparison for industrial purposes. Therefore, the values listed in Table 2 apply to 1 atm. At a pressure of 1 atm, Spencer et al.[15] reported a conversion of 45% at a flow rate of 1 l/min, and an energy efficiency of 20% at a flow rate of 16 l/min, for a microwave discharge, which is still much better than obtained for a DBD.

Another very promising discharge type for CO_2 splitting is a gliding arc plasma, where high flow rates are possible at atmospheric conditions, together with high energy efficiency and reasonable conversion[8,16]. Nunally et al.[8] reported conversions of 2-9% for a SEI variation from 0.1 to 1.0 eV/molecule and flow rate input variation in the range of 14-40 l/min. Furthermore, a maximum energy efficiency of 43 % was reached at a flow rate of 27 l/min. Indarto et al.[16] obtained conversions of 15-18% at a flow rate of 0.8 to 2.4 l/min, but they did not report the energy efficiency as defined by Fridman[7]. However, they compared the power efficiency with a DBD and found that the power efficiency increased with a factor of 3 compared to the DBD described in Wang et al.[37]

We can also compare the plasma-based CO_2 splitting with classical thermal splitting in membrane reactors. In this case, high temperatures of 1400-1800 °C need to be used.[63] This illustrates the advantages of plasma technology, because it can circumvent the difficult thermodynamics of this reaction. Indeed, a high temperature is not needed, because the electrons are heated by the electric power, and they induce the chemical reactions, while the gas itself can remain at or near room temperature. On the other hand, processing at high temperature can also have benefits, when coupling the thermal process with a secondary process. For instance, Jin et al.[64] proposed the coupling of CO_2 splitting and partial oxidation of methane in a membrane reactor, in such a way that the O_2 produced in the splitting diffuses to the second reactor for the partial oxidation process. This method allows the transfer of thermal energy to the membrane and to the partial oxidation process. Although this process still suffers from problems like instability of the membrane, sealing and pressure drop, it shows promising results. If the stability of such membranes can be improved, new possibilities can be found, e.g., in the coupling of a plasma reactor with a partial oxidation reactor, especially for gliding arc and microwave discharges, as they operate at a higher temperature.

Finally, we also looked at photo- and electro-catalytic processes, but it was impossible to compare them with plasma technology, in terms of conversion and energy efficiency. We believe that also here a combination of different processes, like the thermochemical cycle based on Zn/ZnO[65,66] or the

photochemical reduction of CO_2 [67] might give rise to the most valuable process.

Table 2: Benchmark of our results, in terms of maximum conversion, energy efficiency and the corresponding gas flow rates in both cases, with data from literature for other plasma types and classical thermal splitting, all carried out at atmospheric pressure.

	Max. conversion (%)	Flow rate (l/min)	Max. energy efficiency (%)	Flow rate (l/min)
Our work	35	0.01	8	0.5
DBD[1]	30	0.05	-	-
DBD[2]	12.5	0.04	3.5	0.04
Microwave plasma [15]	45	1	20	16
Gliding arc plasma[12]	9	14	43	27
Gliding arc plasma[24]	18	0.8	-	-
Thermal splitting[68]	22	0.02	(1400°C-1800°C)	-

Hence, we can conclude that a DBD reactor can split CO_2 at relatively high conversion, when using a low flow rate, but the energy efficiency is still too low for commercial applications. Indeed, when the electric energy for the CO_2 splitting would originate from fossil fuels, an energy efficiency of 52% would be needed to make sure that not more electric energy is consumed for this process than the electricity produced from the fossil fuel combustion, or in other words, that not more CO_2 is produced in the electricity production than can be split by the plasma process[9].

It should be noted, however, that all the DBD data reported in Table 2, are for simple DBD reactors with a pure CO_2 gas flow, like applied in our study. However, there is still considerable room for improvement for the DBD technology, as already demonstrated in literature[2–6,37,39,40]. Indeed, Figure 14 presents an overview of different modifications applied to DBD reactors, reported in literature, showing both the absolute values of the conversion and energy efficiency reached, as well as the relative changes compared to their standard setup without the modification or with a less efficient modification. Because it is difficult to compare the absolute values of conversion and energy efficiency adopted from literature (due to the different operating conditions and geometries, which are not always thoroughly described), we should mainly focus on the relative changes as a result of these reactor modifications. Note that the relative changes for conversion and energy efficiency were calculated for the conditions of the highest conversion and maximum energy efficiency, respectively.

A packed bed DBD configuration with spherical pellets was proposed by Yu et al.[2]. The authors used silica gel, quartz, γ-Al_2O_3, α-Al_2O_3 and $CaTiO_3$ as packing material and found that the maximum conversion (i.e., 20.5%) was reached for $CaTiO_3$, which was a factor 1.3 higher than for a non-packed DBD. Furthermore, the highest energy efficiency of 6% was obtained for $CaTiO_3$, which was reported at least a factor 1.6 higher than for the non-packed DBD at the same conditions. This packing effect was attributed to the enhancement of the electron energy, thus facilitating the electron impact dissociation of CO_2. Also the morphology and the acid–base properties of the packing material were found to affect the conversion. Furthermore, the presence of heterogeneous reactions on the packing surface was also identified and could facilitate the conversion. It is worth to mention that introducing a dielectric packing in a DBD reactor was also demonstrated to enhance the energy efficiency for VOC remediation[69–72], so we indeed believe that a packed bed DBD reactor has great potential for CO_2 splitting as well.

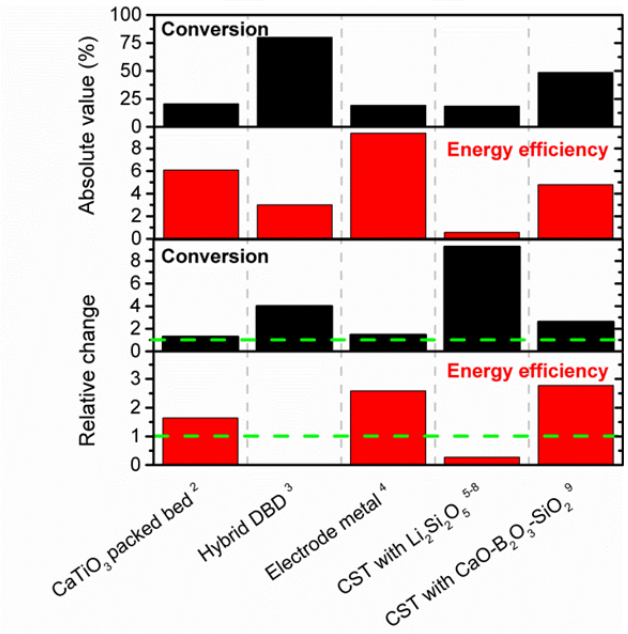

Figure 14: *Modifications to a simple DBD reactor, as reported in literature, yielding a higher CO_2 conversion and energy efficiency. Both the reported maximum values of conversion and energy efficiency are plotted, as well as the relative changes compared to the same setup without the modification. See text for more explanation.The dashed green line indicates no change compared to the standard setup.*

Tagawa et al.[3] proposed a hybrid reactor, i.e., a DBD plasma on the surface of a solid oxide electrolyser cell (SOEC), which allows the in-situ exclusion of O_2 during the CO_2 splitting. A maximum energy efficiency of 3% was reported, but we were not able to deduce the relative change of this parameter in their work. Moreover, an increase with a factor 4 was observed for the conversion, up to a maximum value of 80% compared to the DBD discharge only. Indeed, a high O_2 concentration has a suppressing effect on the CO_2 conversion due to its high electronegativity, thereby trapping the electrons, so that they are not available for electron impact dissociation anymore. Moreover, the oxygen will also be partially present as O atoms, which can react with CO to produce CO_2 (see section 2.2 above). Therefore, it is logical that the in-situ exclusion of O_2 has a beneficial effect on the CO_2 conversion.

Wang et al.[37] investigated the effect of different metals used as high voltage electrode in a DBD reactor for a mixture of 4% CO_2 in helium. The advantage of using different metals as central electrode is that the conductivity of the electrode changes. They obtained a relative order of

Cu≈Au>Rh>Fe≈Pd≈Pt for the reactivity toward CO_2 decomposition, which is the same order as for the electrical conductivity. A maximum conversion of 19.4% was reported for a Cu electrode, while the conversions for Au, Rh, Pt, Fe and Pd were 19.2%, 15.3% 14.2%, 13.2% and 12.9%, respectively. Note again that we should not focus too much on these absolute values, as they were obtained for other conditions (e.g., in a mixture with helium). However, the relative changes are very interesting. Indeed, the Cu and Au electrodes yielded a relative increase in the conversion of a factor 1.5, compared to a Fe (stainless steel) or Pd electrode. Furthermore, a maximum energy efficiency of 9.3% was reported for the Au electrode, which was almost three times higher than the energy efficiency for the Rh electrode at the same conditions. Furthermore, we should point out that the plasma power varies between the electrodes and therefore the energy efficiency is the highest for Au and not for Cu. The maximum energy efficiencies for the Cu, Fe, Pd, Pt and Rh electrodes were 8.5%, 6.7%, 5.9% and 5.6% and 3.6%, respectively.

Li et al.[4,5,39,40] investigated the influence of $Ca_{0.8}Sr_{0.2}TiO_3$ (CST) with 0.5 wt% $Li_2Si_2O_5$ as dielectric barrier, in a mixture of 10% CO_2 in N_2. They found an improvement of the conversion by a factor 9 up to 18.5% at the same electrical power, compared to silica glass as dielectric barrier. However, if the plasma power is taken into account to calculate the theoretical energy efficiency, a drop of the energy efficiency by a factor 0.3 was found, compared to silica glass. The authors concluded that for the same electrical power a much higher plasma power was deposited in the plasma by changing the dielectric barrier, so the actual energy efficiency is in this case closer to the theoretical energy efficiency, which was, however, only 0.6% at its maximum.

In a similar work performed by Wang et al.[6] the performance of a CST ceramic dielectric barrier with glass addition on the conversion of CO_2 was investigated. The authors produced CST ceramic barriers with addition of $CaO–B_2O_3–SiO_2$ (CBS) glass in the range between 0.5 and 5.0 wt%, to enhance the dielectric properties and the microstructures of the ceramics. The experiments were performed in a mixture of 10% CO_2 in N_2. The addition of 5.0 wt% CBS resulted in a rise of the conversion with a factor 2.6 up to 49%, compared to 0.5 wt% CBS. Furthermore, the energy efficiency almost tripled at 5.0 wt% CBS compared to 0.5 wt% CBS, resulting in a maximum of 5%. The authors claimed that a higher amount of CBS leads to a drop in the total surface resistance and a rise in the capacitance of the grain boundaries, which results in a higher CO_2 conversion and a higher energy efficiency. In addition, they also found that the grain boundaries on the dielectric barrier surface serve as charge trapping sites, so that a more homogenous discharge is created.

In summary, although the absolute energy efficiencies reported in these papers are modest, the relative increase in the energy efficiencies due to these modifications, compared to a standard setup or other modifications, is quite promising. Therefore, a combination of the proposed modifications with the proper tuning of the operating parameters might lead to even higher energy efficiencies and possibly could make a DBD reactor competitive with the other plasma systems listed in Table 2.

On the other hand, it is important to realize that more and more electric energy is nowadays originating from sustainable energy sources, and this trend will definitely continue in the coming years. In that case, the energy efficiency requirements of the plasma conversion will be somewhat less strict. Moreover, sustainable energy sources often suffer from peak currents (e.g., on sunny or windy days), when the electricity is in principle “for free”. A DBD plasma can then be very useful for peak shaving, as it is very flexible and can be very easily switched on and off, so that it will be extremely suitable for temporal energy storage.

In general, in terms of practical use, a DBD has some benefits compared to the other plasma types (microwave and gliding arc), because its construction is very simple, robust and allows an easy scale-up, as was already demonstrated 150 years ago for the commercial application of O_3 production[7,60]. Moreover, it is reported in literature that by combining a DBD with a catalyst, in so-called plasma catalysis[73–75], the selectivity of the process can be steered towards the desired products. This is not really an issue for pure CO_2 splitting, but it is very promising when adding a co-reagent (e.g., methane or water), to produce value-added compounds, such as syngas, methanol, formaldehyde and formic acid [46,73,76].

Conclusions

We investigated in detail the effect of various operating conditions on the conversion and energy efficiency of CO_2 splitting in a DBD plasma reactor. The applied frequency and the kind of dielectric (quartz or alumina) seem to have no effect on the conversion and energy efficiency. The discharge gap can have a significant effect when it gives rise to a different streamer behavior. This was indeed observed for the gap of 3.3 mm, compared to the gaps of 1.8 and 2.3 mm, as visualized by the Lissajous plots and the current waveforms. Indeed, the 3.3 mm gap results in less streamer formation, so that the effective plasma (streamer) volume, which can contribute to the CO_2 conversion, is much smaller than the actual reactor plasma volume, resulting in a significantly lower CO_2 conversion and energy efficiency, for the same SEI.

The SEI obviously is most dominant in determining the conversion and energy efficiency. The conversion clearly increases, while the energy efficiency decreases, with rising SEI, which is logical. The SEI itself is determined by both the plasma power and the gas flow rate. We observed that the gas flow rate, and hence the residence time, has the most important effect on the conversion and energy efficiency. The power also has some effect, but it is less significant. Indeed, a higher power with higher gas flow rate gives rise to more intense streamers, but the residence time is lower, and the latter seems more important as it determines the time that the CO_2 molecules stay within the streamers and can be subject to conversion. Therefore, a lower power with lower gas flow rate results in a higher conversion and energy efficiency than a higher power with higher gas flow rate, at the same fixed SEI. This can be of interest, because it means

that a proper tuning of power versus gas flow rate can increase the conversion and energy efficiency at a certain SEI. However, we observed this behavior only for high values of SEI (above 100 J/cm³), which unfortunately yield a low energy efficiency. The effect of the various parameters on the conversion and energy efficiency is summarized in Table 3.

Table 3: Summary of the experimental parameter screening, illustrating their effect on the CO_2 conversion and energy efficiency

Parameter	Effect on conversion	Effect on energy efficiency
Lower gas flow rate/higher residence time	↑↑	↓↓
Higher power	↑	↓
Larger gap (when streamer formation ↓)	↓	↓
Higher frequency	-	-
Dielectric (alumina/quartz)	-	-

The highest CO_2 conversion was found to be around 35%, and was obtained at a high SEI (above 200 J/cm^3), and thus it corresponds to a low energy efficiency of only 2%. On the other hand, the highest energy efficiency, i.e., 8%, was obtained at low SEI (~ 25 J/cm^3), but at the expense of the conversion, which was only a few % in this case. The selectivities of the formed products (i.e., CO and O_2) were also measured, but they were always found to be around 50%, for all conditions investigated.

Besides the experimental results, we have also presented modeling results for the CO_2 splitting, and reasonable agreement was obtained between the calculated and measured conversions and energy efficiencies as a function of SEI, when the power density (and hence the SEI) in the model was multiplied with a factor 7, to account for the smaller volume occupied by the streamers, compared to the total plasma reactor volume.

As the model shows good correlation with the experimental trends, it can be used to elucidate the most important chemical reactions for the CO_2 splitting. For this purpose, we have reduced the chemistry set of our complete model to a more simple model with only 9 species and 17 reactions, to better identify the critical reactions. It was found that the CO_2 splitting is mainly dictated by electron impact dissociation (to form CO and O atoms), electron impact ionization (to form CO_2^+ ions, which will subsequently recombine with electrons or O_2^- ions into CO and O or O_2), and electron dissociative attachment (to form CO and O^- ions). The CO molecules can recombine with O^- ions or O atoms to form again CO_2, but these reactions are only important at high oxygen densities or high conversions (i.e. long residence time). The O atoms can, however, easily recombine into O_2 by a three-body reaction, although a fraction also recombines into O_3. Furthermore, there are also several other reactions between O, O_2 and O_3. Therefore, most freedom to influence the splitting process can be found in the balance of $O/O_2/O_3$.

Finally, we have compared our experimental results for the CO_2 splitting in a DBD with literature data for several types of plasma reactors, as well as with classical thermal CO_2 splitting, to benchmark our results. We can conclude that a DBD reactor can provide reasonable conversions, but the energy efficiency is still too low for commercial applications, at least when using electricity from fossil fuel combustion. However, in literature, several modifications to a standard DBD reactor have been reported already. We have presented a summary of these reactor modifications from literature, illustrating that they might indeed improve the energy efficiency, as well as the conversion.

Furthermore, when using electricity from sustainable energy sources, the energy efficiency might be somewhat less critical. In this respect, we believe that a DBD plasma can even become very useful in the future, for energy storage of peak currents, as it can be easily switched on and off.

Finally, a DBD reactor is also very promising when combined with catalysis. Indeed, when introducing a catalytic packing in a DBD reactor, the selectivity of the process (in case of a co-reagent like methane or water) can be tuned, which has also great promise for the selective production of value-added chemicals.

Experimental Section

1. Experimental setup

1.1. Plasma reactor

A schematic picture of the experimental setup, both in front view and top view, is shown in Figure 15. The plasma reactor is a tubular DBD reactor, consisting of a dielectric tube and two concentric cylindrical electrodes. The inner electrode is a stainless steel rod, which is grounded. We used several diameters for this inner electrode, i.e., 10, 12 and 13 mm, in order to vary the discharge gap (see below). The outer electrode is a nickel foil, connected to a high voltage power supply, and placed around the dielectric tube. The latter has an inner diameter of 16.54 mm and an outer diameter of 22 mm. We used two types of dielectrics, i.e., alumina and quartz. The length of the total reactor, including inner electrode and dielectric tube is 200 mm, but the length of the nickel mesh electrode was only 90 mm, and the latter defines the length of the discharge plasma.

The CO_2 gas flow to the plasma reactor is regulated by mass flow controllers (EL-flow of Bronkhorst), and can be adjusted between 10 and 1000 ml/min. The temperature of the gas is monitored at the inlet and outlet of the DBD reactor by resistance temperature detectors (Endress-Hauser). The DBD reactor is powered by an AC high-voltage power supply (AFS), providing a maximum peak-to-peak voltage of 40 kV and a variable frequency of 1-90 kHz. The total current is recorded by a Rogowski-type current monitor (Pearson 4100), while a high voltage probe (Tektronix P6015A) is used to measure the applied voltage. Furthermore, to obtain the charge generated in the discharge, the voltage on the external capacitor (10 nF) is measured. Finally, all the electrical signals are sampled by a four-channel digital oscilloscope (PicoScope 6402A) and the

discharge power is measured by means of Lissajous figures (see below).

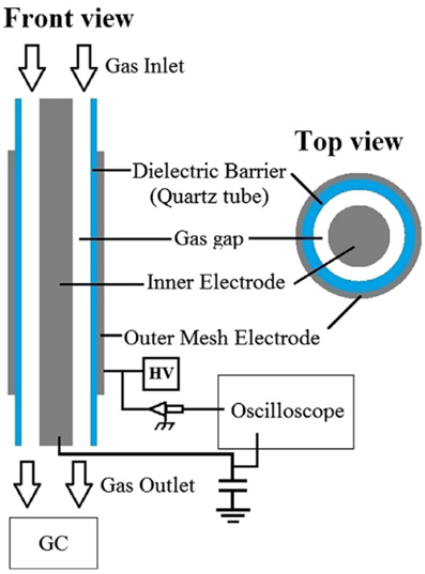

Figure 15: *Schematic diagram of the experimental setup, in front view and top view.*

1.2. Gas analysis

The feed and product gases are analyzed by a three-channel compact-gas chromatograph (CGC) (Interscience), equipped with two thermal conductivity detectors (TCD) and a flame ionization detector (FID). The first TCD channel contains a Molecular Sieve 5A column for the segregation of the molecular gases, O_2, N_2 and CO, while the second TCD channel is equipped with a Rt-QBOND column for the measurement of CO_2 and C_1-C_2 hydrocarbons. The FID is equipped with a Rtx-5 column for the measurement of C1 to C10 containing compounds.

The conversion of CO_2 is calculated from the peak areas measured in the gas chromatograms (where $CO_{2,inlet}$ is measured without plasma):

$$X_{CO_2}(\%) = \left(\frac{CO_{2,inlet} - CO_{2,outlet}}{CO_{2,inlet}} \right) * 100\% \quad \text{(E5)}$$

The oxygen-based selectivities of CO and O_2 are calculated as:

$$S_{CO}(\%) = 0.5 * \frac{CO_{outlet}}{CO_{2,inlet} - CO_{2,\,outlet}} * 100\% \quad \text{(E6)}$$

$$S_{O_2}(\%) = \frac{O_{2,outlet}}{CO_{2,\,inlet} - CO_{2,\,outlet}} * 100\% \quad \text{(E7)}$$

In order to calculate the energy cost and energy efficiency of the process, we first define the specific energy input (SEI) in the plasma from the power and the gas flow rate:

$$SEI\left(\frac{J}{cm^3}\right) = SEI\left(\frac{kJ}{l}\right) = \frac{Power\ (kW)}{Flow rate\ (\frac{l}{min})} * 60(\frac{s}{min}) \quad \text{(E8)}$$

The energy cost to produce 1 mole of CO is then calculated as:

$$E_{CO}\left(\frac{kJ}{mol}\right) = SEI\left(\frac{kJ}{l}\right) * \left[\frac{molar\ volume\left(\frac{l}{mol}\right) * 100\%}{X_{CO_2}(\%)} \right] \quad \text{(E9)}$$

And finally, the energy efficiency (η) is calculated as:

$$\eta(\%) = \frac{\Delta H_R\left(\frac{kJ}{mol}\right)}{E_{CO}\left(\frac{kJ}{mol}\right)} * 100\% \quad \text{(E10)}$$

where the value of the reaction enthalpy (ΔH_R) is 279.8 kJ/mol (see Introduction).

A critical remark should be made when performing inline GC analysis on plasma gas processing. When using an external calibration method, the quantities of the gas components are defined as a function of the molar flow rate of each species. However, the latter changes during the conversion, mainly due to chemical reactions and possibly also due to deposition at the reactor walls. Pinhão and co-workers estimated an expansion (contraction) factor α for mixtures of $He/CH_4/CO_2$ between 0.98 and 1.12[27]. The introduction of noble gases in the gas mixture would allow for an internal calibration, which takes this variation in molar flow rate into account. However, we are interested in the CO_2 conversion without the influence of a noble gas as internal standard. Therefore, in this work, external standards are used, but to account for this expansion effect, we correct, for each specific conversion, for the change in volume due to the change in total number of moles. More specifically, for the reaction under study ($CO_2 \rightarrow CO + 0.5\ O_2$), this means e.g., at 10% conversion, that the gas mixture contains 90 vol% CO_2, 10 vol% CO and 5 vol% O_2, which amounts to a total of 105 vol%. So we multiply by 105% to correct for this change in volume. Of course, this assumes that no other products than CO and O_2 are formed. These are indeed the only products detected on the GC.

2. Description of the model

The calculations were performed with a zero-dimensional (0D) chemical kinetics model, called Global_kin, developed by Kushner and coworkers[77]. It calculates the spatially averaged densities of all plasma species as a function of time, based on a

large number of production and loss terms, as defined by the chemical reactions. The electron temperature is calculated with an energy balance equation and the rate coefficients for electron impact reactions are calculated with a Boltzmann solver. 8 different neutral species (i.e., CO_2, CO, C_2O, C_2, C, O_2, O_3 and O), 11 different positive ions, 6 different negative ions, as well as the electrons are taken into account in the model. Furthermore, several excited levels of CO_2, CO and O_2, are considered, as explained in detail in Aerts et al.[10]. Hence, in total, the model consists of 42 different chemical species, which react with each other in 501 chemical reactions, including electron-impact reactions, ion-ion, ion-neutral and neutral-neutral reactions.

The equations used in the model, the entire reaction chemistry for CO_2 splitting, as well as the approach to mimic the filamentary character of a DBD, were published in[10,59]. However, in the latter work we focused on the detailed plasma chemistry in one microdischarge pulse (of 30 ns) and its afterglow, as well as five consecutive pulses, but no simulations were performed yet for real residence times in the reactor. In the present paper, we apply this model to exactly the same residence times as obtained in the experiments, i.e., in the order of 1-60 s. This means that up to 2000 consecutive pulses (of 60 ns) are simulated, with interpulse time of 0.029 s (34.4 Hz), to mimic the filamentary character of the DBD, i.e., the gas molecules pass through a large number of microdischarge filaments on their way through the reactor. Note that the time between two filaments, as "experienced" by the gas molecules, is not known. Therefore, we have selected an interpulse time of 0.029 s, because it yields reasonable agreement with the experiments for the conversion versus residence time. Moreover, it avoids that the plasma species would accumulate to unphysically high densities in subsequent pulses, which would influence the conversion if the interpulse time was too short. Furthermore, we have chosen the pulse duration to be 60 ns instead of 30 ns, because this will reduce the total number pulses required for the same SEI, and thus it reduces the calculation time. As the actual plasma volume (i.e., sum of the filament volumes) is much smaller than the total volume of the plasma reactor, the deposited energy density in the model needs to be typically a factor 10-100 higher, depending of the gas and reactor geometry under study (i.e., filamentary character or not), to account for this smaller volume[48,49]. In our case, the deposited energy was chosen a factor 7 higher (see section 2).

Finally, we have also developed a reduced chemistry set, by comparing the calculation results with the full set, in the entire range of conditions investigated here, as will be explained below. This reduced set can be very useful for more time-consuming 2D or 3D plasma models of CO_2 splitting.

Acknowledgements

The authors acknowledge financial support from an IOF-SBO project of the University of Antwerp and from the IAP/7 (Inter-university Attraction Pole) program 'PSI-Physical Chemistry of Plasma-Surface Interactions, financially supported by the Belgian Federal Office for Science Policy (BELSPO). The calculations were performed using the Turing HPC infrastructure at the CalcUA core facility of the Universiteit Antwerpen, a division of the Flemish Supercomputer Center VSC, funded by the Hercules Foundation, the Flemish Government (department EWI) and the Universiteit Antwerpen. Finally, we are very grateful to M. Kushner and group members for providing the Global_kin code.

Keywords: Energy conversion; CO_2 splitting; conversion; plasma; Dielectric barrier discharges (DBD)

References

[1] S. Paulussen, B. Verheyde, X. Tu, C. De Bie, T. Martens, D. Petrovic, A. Bogaerts, B. Sels, *Plasma Sources Sci. Technol.* **2010**, *19*, 034015.
[2] Q. Yu, M. Kong, T. Liu, J. Fei, X. Zheng, *Plasma Chem. Plasma Process.* **2011**, *32*, 153–163.
[3] Y. Tagawa, S. Mori, M. Suzuki, I. Yamanaka, T. Obara, J. Ryu, Y. Kato, *Kagaku Kogaku Ronbushu* **2011**, *37*, 114–119.
[4] R. Li, Q. Tang, S. Yin, T. Sato, *J. Phys. D. Appl. Phys.* **2007**, *40*, 5187–5191.
[5] R. Li, Q. Tang, S. Yin, T. Sato, *Appl. Phys. Lett.* **2007**, *90*, 131502.
[6] S. Wang, Y. Zhang, X. Liu, X. Wang, *Plasma Chem. Plasma Process.* **2012**, *32*, 979–989.
[7] A. Fridman, *Plasma Chemistry*, Cambrigde University Press, New York, **2008**.
[8] T. Nunnally, K. Gutsol, A. Rabinovich, A. Fridman, A. Gutsol, A. Kemoun, *J. Phys. D. Appl. Phys.* **2011**, *44*, 274009.
[9] L. F. Spencer, A. D. Gallimore, *Plasma Chem. Plasma Process.* **2010**, *31*, 79–89.
[10] R. Aerts, T. Martens, A. Bogaerts, *J. Phys. Chem. C* **2012**, *116*, 23257–23273.
[11] M. Tsuji, T. Tanoue, K. Nakano, Y. Nishimura, *Chem. Lett.* **2001**, *30*, 22–23.
[12] A. Vesel, M. Mozetic, A. Drenik, M. Balat-Pichelin, *Chem. Phys.* **2011**, *382*, 127–131.
[13] A. P. H. Goede, W. A. Bongers, M. G. Graswinckel, R. M. C. . van de Sanden, L. Martina, K. Jochen, A. Schulz, W. Mathias, *3rd Eur. Energy Conf. Budapest* **2013**.
[14] A. Indarto, J. Choi, H. Lee, H. K. Song, *Environ. Eng. Sci.* **2006**, *23*, 1033–1043.
[15] L. F. Spencer, A. D. Gallimore, *Plasma Sources Sci. Technol.* **2013**, *22*, 015019.
[16] A. Indarto, D. R. Yang, J.-W. Choi, H. Lee, H. K. Song, *J. Hazard. Mater.* **2007**, *146*, 309–15.
[17] M. Kraus, B. Eliasson, U. Kogelschatz, A. Wokaun, *Phys. Chem. Chem. Phys.* **2001**, *3*, 294–300.
[18] Q. Wang, B.-H. Yan, Y. Jin, Y. Cheng, *Plasma Chem. Plasma Process.* **2009**, *29*, 217–228.
[19] Q. Wang, H. Shi, B. Yan, Y. Jin, Y. Cheng, *Int. J. Hydrogen Energy* **2011**, *36*, 8301–8306.
[20] J. Sentek, K. Krawczyk, M. Młotek, M. Kalczewska, T. Kroker, T. Kolb, A. Schenk, K.-H. Gericke, K. Schmidt-Szałowski, *Appl. Catal. B Environ.* **2010**, *94*, 19–26.
[21] I. Istadi, N. Amin, *Chem. Eng. Sci.* **2007**, *62*, 6568–6581.
[22] Q. Wang, B.-H. Yan, Y. Jin, Y. Cheng, *Energy & Fuels* **2009**, *23*, 4196–4201.
[23] H. J. Gallon, H. Kim, X. Tu, J. C. Whitehead, *Energy* **2011**, *39*, 2176–2177.
[24] H. J. Gallon, X. Tu, J. C. Whitehead, *Plasma Process. Polym.* **2012**, *9*, 90–97.
[25] X. Tu, H. J. Gallon, M. V Twigg, P. A. Gorry, J. C. Whitehead, *J. Phys. D. Appl. Phys.* **2011**, *44*, 274007.
[26] X. Tao, M. Bai, X. Li, H. Long, S. Shang, Y. Yin, X. Dai, *Prog. Energy Combust. Sci.* **2011**, *37*, 113–124.
[27] N. R. Pinhão, A. Janeco, J. B. Branco, *Plasma Chem. Plasma Process.* **2011**, *31*, 427–439.
[28] G. Scarduelli, G. Guella, D. Ascenzi, P. Tosi, *Plasma Process. Polym.* **2011**, *8*, 25–31.
[29] C. De Bie, T. Martens, J. van Dijk, S. Paulussen, B. Verheyde, S. Corthals, A. Bogaerts, *Plasma Sources Sci. Technol.* **2011**, *20*, 024008.

[30] R. Snoeckx, R. Aerts, X. Tu, A. Bogaerts, *J. Phys. Chem. C* **2013**, *117*, 4957–4970.
[31] B. Fidalgo, a Dominguez, J. Pis, J. Menendez, *Int. J. Hydrogen Energy* **2008**, *33*, 4337–4344.
[32] Z. Bo, J. Yan, X. Li, Y. Chi, K. Cen, *Int. J. Hydrogen Energy* **2008**, *33*, 5545–5553.
[33] M. Kano, G. Satoh, S. Iizuka, *Plasma Chem. Plasma Process.* **2011**, *32*, 177–185.
[34] U. Kogelschatz, *Plasma Chem. Plasma Process.* **2003**, *23*, 1–46.
[35] S. Futamura, H. Kabashima, *Carbon Dioxide Utilization for Global Sustainability, Proceedings of 7ththe International Conference on Carbon Dioxide Utilization*, Elsevier, **2004**.
[36] A. Gutsol, A. Rabinovich, A. Fridman, *J. Phys. D. Appl. Phys.* **2011**, *44*, 274001.
[37] J. Wang, G. Xia, A. Huang, S. L. Suib, Y. Hayashi, H. Matsumoto, **1999**, *159*, 152–159.
[38] G. Zheng, J. Jiang, Y. Wu, R. Zhang, H. Hou, *Plasma Chem. Plasma Process.* **2003**, *23*, 59–68.
[39] R. Li, Q. Tang, S. Yin, T. Sato, *Fuel Process. Technol.* **2006**, *87*, 617–622.
[40] R. Li, *Solid State Ionics* **2004**, *172*, 235–238.
[41] H.-H. Kim, a. Ogata, *Eur. Phys. J. Appl. Phys.* **2011**, *55*, 13806.
[42] D. R. Lide, W. M. M. Haynes, G. Baysinger, L. I. Berger, D. L. Roth, D. Zwillinger, M. Frenkel, R. N. Goldberg, *J. Am. Chem. Soc.* **2009**, *131*, 12862–12862.
[43] R. Valdivia-Barrientos, J. Pacheco-Sotelo, M. Pacheco-Pacheco, J. S. Benítez-Read, R. López-Callejas, *Plasma Sources Sci. Technol.* **2006**, *15*, 237–245.
[44] K. F. Young, H. P. R. Frederikse, *J. Phys. Chem. Ref. Data* **1973**, *2*, 313.
[45] K. Francke, R. Rudolph, H. Miessner, *Plasma Chem. Plasma Process.* **2003**, *23*, 47–57.
[46] D. Larkin, *Catal. Today* **2001**, *71*, 199–210.
[47] A. A. Khassin, B. L. Pietruszka, M. Heintze, V. N. Parmon, *React. Kinet. Catal. Lett.* **2004**, *82*, 111–119.
[48] O. Motret, C. Hibert, S. Pellerin, J. M. Pouvesle, *J. Phys. D. Appl. Phys.* **2000**, *33*, 1493–1498.
[49] O. Motret, S. Pellerin, M. Nikravech, *Plasma Chem. Plasma Process.* **1997**, *17*, 393–407.
[50] T. Kozák, A. Bogaerts, *Plasma Sources Sci. Technol.* **2014**, *23*, 045004.
[51] T. G. Beuthe, J.-S. Chang, *Jpn. J. Appl. Phys.* **1997**, *36*, 4997–5002.
[52] A. Cenian, A. Chernukho, V. Borodin, *Contrib. to Plasma Phys.* **1995**, *35*, 273–296.
[53] A. A. Ionin, I. V Kochetov, A. P. Napartovich, N. N. Yuryshev, *J. Phys. D. Appl. Phys.* **2007**, *40*, R25–R61.
[54] H. Hokazono, H. Fujimoto, *J. Appl. Phys.* **1987**, *62*, 1585.
[55] H. Hokazono, M. Obara, K. Midorikawa, H. Tashiro, *J. Appl. Phys.* **1991**, *69*, 6850.
[56] S. Hadj-Ziane, B. Held, P. Pignolet, R. Peyrous, C. Coste, *J. Phys. D. Appl. Phys.* **1992**, *25*, 677–685.
[57] A. Cenian, A. Chernukho, V. Borodin, G. Śliwiński, *Contrib. to Plasma Phys.* **1994**, *34*, 25–37.
[58] W. Tsang, R. F. Hampson, *J. Phys. Chem. Ref. Data* **1986**, *15*, 1087–1279.
[59] R. Aerts, R. Snoeckx, A. Bogaerts, *Plasma Process. Polym.* **2014**, *11*, 985–992.
[60] B. Eliasson, M. Hirth, U. Kogelschatz, *J. Phys. D. Appl. Phys.* **1987**, *20*, 1421–1437.
[61] M. Ramakers, I. Michielsen, R. Aerts, V. Meynen, A. Bogaerts, **n.d.**, unpublished work.
[62] A. Gutsol, A. Rabinovich, A. Fridman, *J. Phys. D. Appl. Phys.* **2011**, *44*, 274001.
[63] S. Rayne, *Nat. Preced.* **2008**, DOI: 10.1038/npre.2008.1741.1.
[64] W. Jin, C. Zhang, P. Zhang, Y. Fan, N. Xu, **2006**, *52*, 0–5.
[65] M. E. Gálvez, P. G. Loutzenhiser, I. Hischier, A. Steinfeld, *Energy & Fuels* **2008**, *22*, 3544–3550.
[66] P. G. Loutzenhiser, M. E. Gálvez, I. Hischier, A. Stamatiou, A. Frei, A. Steinfeld, *Energy & Fuels* **2009**, *23*, 2832–2839.
[67] R. D. Richardson, E. J. Holland, B. K. Carpenter, *Nat. Chem.* **2011**, *3*, 301–3.
[68] Y. Nigara, B. Cales, *Bull. Chem. Soc. Jpn.* **1986**, *59*, 1997–2002.
[69] H. L. Chen, H. M. Lee, S. H. Chen, *Ind. Eng. Chem. Res.* **2008**, *47*, 2122–2130.
[70] G. Horvath, N. J. Mason, L. Polachova, M. Zahoran, L. Moravsky, S. Matejcik, *Plasma Chem. Plasma Process.* **2010**, *30*, 565–577.
[71] A. Ogata, K. Mizuno, S. Kushiyama, T. Yamamoto, **1998**, *18*, 363–373.
[72] H.-X. Ding, A.-M. Zhu, X.-F. Yang, C.-H. Li, Y. Xu, *J. Phys. D. Appl. Phys.* **2005**, *38*, 4160–4167.
[73] X. Tu, J. C. Whitehead, *Appl. Catal. B Environ.* **2012**, *125*, 439–448.
[74] K. Francke, *Catal. Today* **2000**, *59*, 411–416.
[75] H. Chen, H. Lee, S. Chen, Y. Chao, M. Chang, *Appl. Catal. B Environ.* **2008**, *85*, 1–9.
[76] T. Nozaki, K. Okazaki, *J. Japan Pet. Inst.* **2011**, *54*, 146–158.
[77] R. Dorai, M. J. Kushner, *J. Appl. Phys.* **2000**, *88*, 3739–3747.